Title
Environmental challenge rewires functional connections among human genes

Author
Herken, Benjamin Whitman

Publication Date
2023

Environmental challenge rewires functional connections among human genes

by
Ben Herken

DISSERTATION
Submitted in partial satisfaction of the requirements for degree of
DOCTOR OF PHILOSOPHY

in

Genetics

in the

GRADUATE DIVISION
of the
UNIVERSITY OF CALIFORNIA, SAN FRANCISCO

Approved:

DocuSigned by:
David Toczyski
B39DA64A208E4CB...

David Toczyski

Chair

DocuSigned by:
Bjoern Schwer

Bjoern Schwer

DocuSigned by:
LUKE GILBERT
71F73C69F83C48B...

LUKE GILBERT

Committee Members

Dedicated to my parents for their immeasurable love and support.
Gregg Franklin Herken
Linda Aven Switzer

It is impossible to say just what I mean!
But as if a magic lantern threw the nerves in patterns on a screen.
The Love Song of J. Alfred Prufrock, T.S. Eliot

Environmental challenge rewires functional connections among human genes

Benjamin Herken

ABSTRACT

A fundamental goal of biology is understanding how a limited number of human genes are responsible for governing the cellular response to myriad insults and environmental changes. Relationships between genes, processes, and ontologies are thought to be necessarily plastic to achieve this adaptability, but quantitative determination of gene functional connection is non-trivial and historically difficult at scale. Here, we developed a framework for conditional genetic interaction mapping in human cells to evaluate the plasticity of human genetic architecture upon environmental perturbation using three distinct challenges to cell cycle regulation, genome fidelity, and metabolism as archetypes. For the first time, we systematically and quantitatively discover rewiring of human gene functional connections across conditions, shedding light on how interdependence of ontologies is contingent on their environment. We reproducibly nominate novel context specific complex identities, and propose new putative relationships between established complexes and individual genes. This concept is highlighted in our finding that the TIP60 histone acetyltransferase complex radically alters its interaction profile after inhibition of ATR, moving from a peripheral to a key factor in the regulation of core cellular processes such as cell cycle control and metabolism. We further find that loss of TIP60 function yields a cell state that is refractory to the effects of ATR inhibition at the transcriptional level. Our work here provides a resource for understanding the genetic landscape regulating DNA replication

fidelity and metabolism and establishes a scalable framework for measuring the plasticity of human gene function in response to environmental stimulus.

TABLE OF CONTENTS

LIST OF FIGURES

INTRODUCTION

Drawing functional connections between individual genes, pathways, and processes can be helpful for understanding the interdependence of ontologies in programming cellular phenotypes. However, teasing apart these reliances is challenging, time consuming, and often leaves an incomplete picture of how bioprocesses function together. Furthermore, most studies that seek to nominate putative associations between genes are limited to the basal environmental condition in which their model system is maintained.

Recently, systems biology approaches have made great progress in assigning function to understudied genes and have provided a wealth of unbiased high-throughput data from which to generate hypotheses (*1*–*4*). One such approach that provides a scalable snapshot of genetic architecture is measuring genetic interaction (GI) between gene pairs. Gene pairs that genetically interact are usually found to be related or are components of distinct biological processes whose cooperation is (sometimes unexpectedly) important for cellular homeostasis (*5*, *6*). GI occurs when a combination of genetic perturbations elicits a phenotype that quantitatively differs from an expectation based on the single gene perturbation effects. Classically, GIs are observed in cell viability experiments, where surprisingly deleterious or mitigated growth defects are classified as either synthetic sick/synthetic lethal (SS/SL) or buffering/epistatic interactions, respectively (*7*–*9*).

GI mapping, in which a large matrix of GIs is systematically and quantitatively measured between sets of genes, enables high-throughput identification of human genetic interactions. In a GI map, each gene's interaction profile can be used as a multi-

dimensional signature to form hierarchical clusters. Clustered genes are often found to exist in protein complexes, have similar roles, or belong to similar ontologies (*10*, *11*). GI mapping has been used successfully in various organisms to assign putative function to unknown genes and discover novel complexes or pathways (*12*). Until recently, technical limitations have precluded large scale measurement of GIs in human cells. The advent of CRISPR-based technology has led to numerous gene deletion, knockdown, and activation screens in human cell culture (*13*–*18*). These CRISPR methods have been extended to map GIs in human cells and also enable prediction of functional connections through data integration and co-correlation analysis (*19*–*22*).

While the utility of these analytic frameworks is well appreciated, one persistent shortcoming in their design is the assumption that gene functionality is more or less static and that these approaches implicitly seek a singular annotation to explain gene behavior. Yet, given our current understanding of the size and structure of the human genome, the number of cell types in a human body, and the environmental challenges that must be adapted to at a cellular and organismal level: a one gene - one function relationship is infeasible in humans. The historical difficulty of molecular genetics has necessitated such reductive reasoning, but this could also underlie contradictions in the literature explainable by context specific phenotypes (*23*, *24*).

In a first attempt to address this shortcoming, a study in yeast has conceptually extended GI mapping to measure the environmental dependencies of genetic interactions at large scale (*25*). In this study, ~30,000 gene-gene perturbations representing diverse cellular ontologies were queried against 14 distinct environmental conditions that include metabolic, genotoxic, and targeted bioactive compounds.

Interactions specific to an environment were evaluated against a reference set of interactions from a genome scale yeast GI map. This data demonstrated that environmental GIs are rare leading the authors to conclude that the reference set of interactions is mostly robust to alteration from environmental stimulus. While this study provides a strong argument for systemic resilience to change, demonstrating that independent ontologies largely remain independent, it remains to be seen if genes that modify the cellular response to a specific environmental challenge might be enriched for rewiring phenotypes *between* those genes. Furthermore, recent comparisons of GI profiles of homologous genes in yeast and worms found a distinct lack of conservation of genetic interactions (*26*). This suggests that even as gene function may be consistent across organisms, the nature of relationships between gene sets cannot be assumed as static. Together, these studies highlight open questions such as how genetic networks respond to and are rewired by changing environments.

We posit that the incongruity between the size of the human genome and the myriad conditions it is tasked with responding to necessitate rewiring phenotypes, where a gene product's function is environmentally dependent. No large-scale experiments have investigated the mutability of genetic functional connections systematically in a human cell. Here, for the first time we use CRISPRi-based GI mapping technologies to investigate genetic rewiring in three environmental contexts: S-phase checkpoint inactivation, genotoxic insult, and glucose starvation. We create two reference and three environmental GI maps using a combination of genotoxic chemicals, bioactive pharmaceuticals, and growth media deprivation to reveal gene by gene (GxG) and gene by gene by environment (GxGxE) interactions. Each GI map

provides an illuminating and distinct snapshot of cellular architecture in each cell state. We find robust and coherent clusterings of genes by function in all maps, however the interactions *between* ontologies are highly context dependent. We observe clusterings of poorly defined genes into new putative complexes, and unpredicted novel GIs between seemingly independent complexes. We measure the highest density of rewired environmental genetic interactions when querying gene pairs that have a primary influence on cellular fitness in the environment in question, as has been suggested by previous studying in yeast.

Rewired genetic interactions measured between genes implicated in the DNA damage response (DDR), cell cycle regulation, and metabolism have potential clinical ramifications, as many of the genes assayed in our experiments have recognized roles in human disease states and the ATR inhibitor we use to induce environmental challenge is currently being evaluated as a potential therapeutic. Cumulatively, this study provides a large dataset of functional connections pertaining to DNA replication fidelity and metabolism and an illuminating first examination of environmentally rewired relationships among human genes.

RESULTS

A nominating CRISPRi screen identifies genes that modify sensitivity to ATR inhibition.

Two landmark studies have systematically measured environmentally triggered genetic rewiring in yeast, however the nature of this feature of cell biology remains unexplored in human cells (*25*, *27*). In yeast, genetic rewiring phenotypes have been found enriched among genes whose perturbation modifies the cellular response to an environmental challenge (*25*). We sought to generate an unbiased list of genes responsible for modifying cellular sensitivity to perturbation of the ATR kinase, a critical regulator of the S-phase DNA damage checkpoint, as a basis to probe rewiring of human gene function. We reasoned that the DNA damage response is a dynamic signaling network which could be enriched for gene functions that can be rewired by environmental perturbations (*28*). To this end, we performed a nominating genome-scale CRISPR interference (CRISPRi) screen in K562 human leukemia cells in presence or absence of the ATR inhibitor AZD6738 (ATRi) using our established screening pipeline (**Fig. 1A**) (**Supplemental Data 1**) (*29*, *30*). A total of 293 genes were found to impart a selective sensitivity or resistance to the ATR inhibitor. Between independent replicates we find highly reproducible sgRNA phenotypes in both the untreated and ATRi treated arms of the experiment (**Fig. 2B, C**).

Importantly, many hallmark genes known to be crucial for ATR function or previously found as strong modulators of the ATRi response were identified in our hit gene list (*31*–*33*). This includes all three members of the 9-1-1 complex (RAD9A, HUS1, RAD1) and its loader RAD17, which appear as the top four genes whose knockdown

leads to increased ATRi sensitivity (**Fig. 1B**). We also find CDC25A, whose loss has an established protective effect against ATRi (*31*, *34*), as our strongest resistance hit. The abundance of positive controls among this list as well as high enrichment of gene ontology (GO) terms relevant to DNA repair, cell cycle, and chromatin regulation provided confidence in using this geneset to generate high quality datasets to map genetic interactions (**Fig. 1C**). In addition to predictable DNA repair and cell cycle regulatory factors, our hit list is populated by various genes with GO annotations not canonically associated with ATR biology (**Supplemental Data 1**). These surprising additions open the possibility of discovering novel interactions between features of cell biology not usually studied together or mediated by direct physical interactions.

Variable condition genetic interaction maps of ATR biology.

We selected the top two scored sgRNAs targeting each hit gene in our nominating screen to clone a pooled dual-sgRNA GI mapping library (**Supplemental Data 2**), as described previously, containing all combinations of sgRNAs (*19*). Our final library is composed of 408,321 pairs of sgRNAs corresponding to 48,828 unique dual-gene perturbations with eight constructs targeting each gene pair (**Fig. 1A**) (**Fig. 3A**).

We performed parallel CRISPRi GI screens in K562 using our dual-sgRNA library under two environmental conditions: normal growth and ATR inhibition. Two biological replicates represent each GI experiment (**Fig. 3B, C**).

Our library generates 52 independent measurements of each single gene perturbation phenotype, by pairing every individual gene targeting sgRNA with a panel of non-targeting negative control (ntc) sgRNAs. This enables high quality determination

of single gene perturbation phenotypes, which is critical for accurate calling of genetic interactions. The single gene phenotypes derived from both GI screens correlate strongly with those calculated in our nominating screen (**Fig. 4A, B**).

A matrix of sgRNA level genetic interactions was produced using an analytic strategy previously employed for GI mapping in mammalian cells (*19*). For each individual sgRNA, a regression model is applied from the distribution of dual-sgRNA phenotypes that includes the query sgRNA and all single sgRNA phenotypes (**Fig. 5A, B**). GIs of sgRNA pairs that include the query sgRNA are then calculated based on the deviation of the observed pair phenotype from the model. The high representation of ntc sgRNAs in our library provides an empirical measurement of noise in our experiments, allowing us to calibrate putative GI scores by normalizing sgRNA level GIs by the standard deviation of the negative control distribution for that specific sgRNA.

Finally, gene level GIs are calculated by averaging all sgRNA level GIs that target the same pair of genes. As interactions calculated from the ATRi treated arm of the screen represent a specific gene by gene by environment phenotype, we refer to them as ATRi environmental Genetic Interaction (eGI) to distinguish from the untreated GI data (Reference GI matrix and ATRi eGI matrix: **Supplemental Data 3 and 4**, respectively).

We find a high degree of correlation between independent experimental replicates for both GI and ATRi eGI maps at the sgRNA and the gene level (**Fig. 5C**). Thresholds were defined as four standard deviations of the negative control distribution to determine significance of GI scores using the distribution of gene-negative control GIs. This analysis yields 292 (0.6%) positive and 782 (1.6%) negative genetic

interactions in the untreated condition and 1127 (2.3%) positive and 2391 (4.9%) negative environmental genetic interactions in the ATRi condition (**Fig. 5D, E**). GIs are assumed to be rare and the density of GIs found in these experiments is similar to that found in other mammalian GI maps (*19*, *35*). We also find that there is no dependency between each gene perturbation's primary growth or drug-treated phenotype and the sign or magnitude of its GI or eGI scores (**Fig. 4C, D**), further bolstering confidence in our experimental and analytic approach.

Importantly, GIs recapitulate established functional relationships, such as the interaction between the BRCA1 and Fanconi Anemia (FA) complexes (**Fig. 5F**) (*36*). Intriguingly, this interaction is not conserved in the ATRi eGI map, suggesting that loss of ATR function might sever the connection between sensing of a lesion and recruitment of effector proteins to manage its repair.

Measuring genetic interactions with essential genes has historically required complicating hybrid approaches to perturbing gene function. Knockdown by CRISPRi enables high quality determination of GI with genes whose function is critical to cellular homeostasis. For instance, robust GI and ATRi eGI profiles were measured for PPP2R1A, a component of the essential Protein Phosphatase 2A (PP2A) complex that is implicated in various control mechanisms to inhibit cell cycle progression. Negative genetic interactions are found between PPP2R1A and WEE1, PKMYT1, and MDC1 - all important checks on ectopic progression into M-phase (*37*, *38*). These negative GIs may be indicative of a compounding failure to regulate cell cycle progression leading to mitotic catastrophe.

Genetic interactions are often found between genes that physically interact with one another, and we were interested in the extent of overlap between interactions from our dataset and canonical protein-protein interactions (PPI). We used the STRING PPI database to determine how effectively our dataset can recall physical interactions. We find gene pairs that exhibit GI or ATRi eGI are enriched for physical interactions relative to all gene pairs in our dataset (**Fig. 5G**). Gene pairs with a significant GI have over three times the average STRING PPI score as all pairs, while pairs interacting in the ATRi condition have twice that average.

Providing further confidence in our analytic framework, a subset of GIs measured in both conditions were validated by fluorescence competition assays. In these assays, perturbed and wild-type cells are grown together, and fitness phenotypes are calculated by monitoring depletion or enrichment of the perturbed cells over time using a fluorescent protein expression as a proxy to mark genetically perturbed cells (**Fig. 6A-D**). Additionally, GIs and ATRi eGIs measured in K562 were conserved in A549 lung cancer cells by fluorescence competition assay, suggesting that at least within DNA replication and S-phase checkpoint biology, cell line specific interactions are likely uncommon (**Fig. 6E-H**).

Differential interactions reveal rewiring of inter-ontology functional connections in ATRi treated cells.

The degree of contrast in interaction abundance between the reference and ATRi eGI maps surprised us and we sought to understand if the large number of interactions measured in the ATRi conditions was due to accentuation of existing phenotypes from

the GI map, or new genetic interaction due to broad rewiring of gene function in the treated condition. The GI and ATRi eGI map scores correlate (R=0.42), but sizable populations of interacting gene pairs are only found in one condition, with 654 and 3021 GIs/eGIs specific to the untreated and environmental datasets, respectively. Many interactions measured in the ATRi eGI map are not detectable in the GI map, even when accounting for variations in signal strength between conditions (**Fig. 7B**).

Differential GIs (dGIs), representing the rewired nature of an interaction across environmental conditions, have not been systematically studied in human cells. We were interested in determining if we could use differences between our GI and eGI datasets to measure rewiring of biological processes. To begin to examine the features of this potential biology, we created a third matrix by taking the difference of each gene pair's score in the ATRi eGI and GI maps. In this matrix, interactions that are refractory to ATRi are removed, and the resulting matrix displays only the extent to which genetic interactions are altered by treatment with ATRi. We observed that dGIs are not random but rather are frequently coherent for genes within annotated protein complexes such as for example the TIP60 complex (BRD8, DMAP1, EP400 and TRRAP) which we will discuss further below (**Fig. 7C**). A null distribution of gene-ntc dGIs was used to set thresholds for effect size and significance. In this case, the threshold was set to five times the standard deviation of the negative control population. We find 514 negative and 200 positive rewired genetic interactions that clear this threshold (**Fig. 7D**).

An expanded set of environmental interaction maps display distinct and coherent genetic rewiring in genotoxic and glucose deprived conditions.

We find our ability to measure rewiring of genetic interactions across environmental conditions robust in the ATRi treated context. Next, we were interested if the scope or specifics of our rewired interactions would be consistent in additional environmental contexts. To this end, we performed another set of GI screens in K562 cells using the same dual-guide library. We grew cell populations in three conditions. A DMSO control condition served as an untreated reference and as a direct experimental replicate to the matched experiment from the first set of screens. Cells were also grown in the presence of the topoisomerase II poison Etoposide, which induces genome toxicity through DSB formation and replication fork collapse. Finally, cells were grown in growth media identical to the other conditions, except without supplemented glucose. These experiments yielded one new reference GI map and two new environmental GI maps (Reference GI Matrix 2, etoposide eGI matrix, glucose deprived eGI matrix: **Supplemental Data 5-7**, respectively).

We find a strong correlation between GI scores measured in the untreated reference map from the first and second set of experiments (R = 0.68) (**Fig. 8A**). However, linear regression of the two datasets (expt. 1 vs expt. 2) yields a slope of 0.59, suggesting the first reference map detected stronger genetic interactions than the follow-up. Indeed, after setting thresholds for significance at four standard deviations of the gene-negative control distribution, we detect 752 interactions in the second GI matrix, fewer than the 1074 interactions measured in the first experiment. In order to measure false discovery of rewired interactions we calculated a difference matrix

between the matched reference maps and set thresholds for significance, as before. We only find 33 “rewired” interactions between the two maps, suggesting that our rate of identifying false positives in differential interactions is very low and providing confidence in our methodology.

Differential interactions were measured between the etoposide treated and matched reference maps. 174 positive and 88 negative dGIs passed our significance threshold in this comparison (**Fig. 8B**). Closer examination of the data revealed that much of the rewiring signature was being driven by a small number of genes. We find two catalytic subunits of the PP2A complex (PPP2R1A, PPP2R2A) form strong differential interactions with several other genes when cells are treated with etoposide (**Fig. 8D**). Loss of PP2A is generally toxic but provides resistance in cells treated with etoposide. We find etoposide treatment specific relationships between PP2A and core regulators of cell cycle progression, transcription, and signal transduction that are distinct from its set of interacting genes under basal conditions (**Fig. 8F**). This set of positive interactions is specific to the etoposide condition, with neither of the reference experiments nor the ATRi or glucose deprived maps recapitulating this relationship, suggesting a relationship unique among these data sets to a cell state marked by exogenous DNA damage.

We sought to apply the same differential analysis to the glucose deprived map. After setting thresholds as before, we measure 112 positive and 43 negative differential interactions in the comparison of the glucose deprived map to its matched reference control (**Fig. 8C**). Similar to the differential set of interactions measured after treatment with etoposide, we find that a small number of genes is influencing this signal. Three

genes known to be necessary for glycolysis as well as a fourth with a very similar profile (see clustering analysis below) are repeatedly found to form strong negative interactions with genes that are important for mitochondrial homeostasis and oxidative phosphorylation. These interactions are reproducible in both reference maps, the ATRi map, and the etoposide map, with little variation. However, in the glucose deprived map, this set of interactions is entirely missing (**Fig. 8G**). This result suggests that, in these cells, the critical interlinked role of these two ontologies in energy utilization is severed. Presumably, in the cell state that results from starving cells of glucose supplemented in the media, the effect of disabling glycolytic genes is negligible.

In both these environmental conditions, DNA damage induced by the genotoxic agent etoposide and glucose deprivation, we find many fewer differential genetic interactions than were measured for the ATRi map. This may reflect that the genes used in the library in each of these screens were selected from the primary growth phenotypes in the presence of the ATR inhibitor. However, we are still able to detect sets of rewired interactions between sets of genes that have a known relationship with the environmental challenge in question. Together, this indicates that rewired genetic interactions are rare but may be enriched among genes that are important on their own to the cellular response to the environment.

Integrated analysis of GI and eGI matrices clusters genes by function.

Clustering genes by the similarity of their interactions with all other genes in each map provides a scalable and quantitative approach for measuring functional connections, as genes with similar GI profiles tend to be involved in similar biological

processes or protein complexes. For ease of visualization and direct comparison we first clustered all five maps (both references, ATRi, etoposide, and glucose deprivation) using a “consensus” method where all GI and eGI scores were first normalized by the variance in their respective populations. Next, for each gene, the normalized GI and eGI profiles were concatenated and this new matrix was used to generate clusters using the average pairwise linkage of the Pearson correlation. This clustering can then be applied to all GI matrices from the reference and environmental conditions (**Fig. 9A-C**). This analysis observes robust groupings of genes with known similar functions. Clusters of as few as two genes reveal cognate binding partners (e.g. the relationships between BRCA2/PALB2 and BRCA1/BARD1). Medium sized clusters of between five and twelve genes outline known complexes such as the TIP60 histone acetyltransferase and Complex I of the electron transport chain. Large clusters of up to one hundred genes tend to associate cellular compartments, like the mitochondria or concerted cellular bioprocesses like homology directed repair.

Predictable clusters are helpful for orienting our understanding of the maps into echelons of biological complexity but are perhaps most interesting when they include understudied genes that cluster with one another or with established complexes, as this allows rapid generation of hypotheses regarding the functions of these genes. Interestingly, we observed that the karyopherin XPO4 clusters closely with the dedicated glycolysis factors GPI, HK2 and ENO1 and all four genes display strong negative GIs with mitochondrial factors involved in oxidative phosphorylation. These interactions were validated by fluorescence competition assay (**Fig. 6C, D**), suggesting

a specific role for nuclear-cytoplasmic translocation in the function of glucose metabolism.

Another example of novel clustering is illustrated in a grouping containing only CCDC6 and FBXO42. CCDC6, a gene which is mostly known for its propensity to fuse with proto-oncogenes in various human malignancies, is also thought to have a role in potentiation of DNA damaging signaling through the phosphorylated histone variant **γ**H2AX, though a direct mechanism for this activity remains unclear (*39*). FBXO42 belongs to a family of genes that provide target specificity to SCF ubiquitin ligase complexes. The cluster negatively interacts in all maps with SCF core and accessory proteins such as CUL1, UBA3, and NEDD8. Both genes also display severe negative interactions with PPP2R1A, indicating that CCDC6 and FBXO42 may be influencing cell cycle progression. Supporting a function for these genes as cell cycle regulators, propidium iodine staining of CCDC6 or FBXO42 perturbed K562 cells show similar cell cycle distributions as wild type cells in unperturbed basal condition. However, upon ATRi, the percentage of CCDC6 or FBXO42 perturbed cells in G1 decreases relative to ntc cells (**Fig. 10A-C**). The clustering of these genes, their interaction profile, and activity influencing cell cycle distribution, indicate that CCDC6 and FBXO42 might serve as a check on progression from G1 phase likely mediated by SCF dependent degradation of target proteins. The perturbation of these genes may trigger further ectopic cycling that negatively synergizes the ATR inhibition to dramatically accelerate the cell cycle, leading to mitotic catastrophe.

The TIP60 HAT complex displays extensively rewired eGIs in ATRi treated cells.

One trend we observed in our data is that many gene pairs with negative eGIs in the ATRi map do not interact under unperturbed conditions. On closer analysis, a striking number of these pairs contain at least one component of the TIP60/NuA4 HAT complex. TIP60 is a highly conserved family of genes with diverse roles primarily in stimulating gene expression, mobilizing the DDR through ATM activation, and facilitating histone variant exchange, particularly H2AZ and H2AX (*40–42*).

Many, but not all, annotated members of TIP60 are present in our dataset (DMAP1, EP400, BRD8, MRGBP, EPC2, and TRRAP) and form a cluster together. (*43*). We were interested in the effects on cell viability from repression of the TIP60 complex across conditions and how this translates to conditionally dependent GIs. A closer look at the TIP60 GI and ATRi eGI profiles show that TIP60 knockdown by itself provides a protective effect against ATRi, as was observed in the nominating screen. However, when TIP60 knockdown is paired with many other sgRNAs, even those that exhibit no phenotype on their own, the dual sgRNA perturbation results in markedly sicker cells. Our data implicate TIP60 as important to the cellular response to replication stress in two important ways. First, loss of TIP60 confers a selective advantage upon inhibition of ATR. Second, S-phase checkpoint inactivation results in a cell state in which TIP60 forms genetic interactions with many key gene sets that themselves modify cell growth in a ATRi specific manner. These interactions tend to be associated with core cellular processes, like regulators of metabolism, gene expression, and cell cycle progression rather than DNA damage specific effectors.

We next investigated if the strong growth and interaction phenotypes observed from loss of TIP60 in the context of ATR inhibition caused similarly unexpected alterations in gene expression, reasoning that TIP60's annotated role as an important regulator of transcription might make it particularly amenable to this type of phenotypic readout. To this end we employed bulk RNA sequencing (RNAseq) to measure genes that are differentially expressed upon knockdown of TIP60. We find that knockdown of either the BRD8 or DMAP1 subunits of TIP60 induce widespread differential gene expression relative to ntc K562 cells in the untreated reference condition, underscoring the importance of this complex. We find considerable overlap in the specific genes that are differentially expressed in these comparisons, indicating that knockdown of either BRD8 or DMAP1 results in similar transcriptomic consequences (**Fig. 11A)**.

We repeated this experiment in A549 cells to understand if we could extrapolate these findings in another cell line and observed a similarly large amount of differential gene expression upon TIP60 perturbation (BRD8 or DMAP1 knockdown) **(Fig. 11B)**. Although differentially expressed genes in the two TIP60 perturbations are less correlated in A549 than the same comparison in K562, this correlation is stronger than that of perturbations between cell lines. Accordingly, the regulation of specific genes between the K562 and A549 arms of the experiment was considerably different. GO term enrichment of genes differentially expressed exclusively in A549 show clear activation of a p53 dependent apoptotic program, with a simultaneous downregulation of key markers of cell growth and homeostasis, including mitotic factors and ribosome biogenesis. In contrast, in K562, which do not have active p53 signaling, we find a

unique transcriptomic signature indicating mobilization of erythroid differentiation, a known response to cellular stress in this cell line (**Fig. 11C, D**).

Treatment of unperturbed K562 with an ATR inhibitor induced changes in gene expression, although not on the scale observed with perturbation of the TIP60 complex (either BRD8 or DMAP1). However, many of the genes found to be differentially expressed are shared with the TIP60 perturbed cells and again indicate activation of a transcriptional network associated with differentiation. In the subset of genes whose expression changes exclusively upon ATRi we observed an upregulation of key cell cycle markers under direct influence of the S-phase checkpoint, such as CDC25A. Importantly, we find in the sgTIP60 exclusive genes a clear downregulation of apoptotic factors such as NFKBIA and numerous metabolic genes such as those involved in fatty acid oxidation and upregulation core histones.

Finally, we compared the effect of perturbing ATR in sgTIP60 cells relative to untreated sgTIP60 cells. We found no significant differential expression of any genes in this comparison (**Fig. 11E-H**). These results suggest that loss of activity of the TIP60 complex may induce a cell state refractory to the effects of S-phase checkpoint inactivation. While surprising that a genetic perturbation could yield cells entirely unsensitized to drugging of an essential cell cycle regulator, this transcriptomic data agrees with the protective effect of sgTIP60 seen in our nominating and GI screen data. These findings support the notion that genetic rewiring (dGIs) can only be captured by comparative analysis of GI and eGI maps and would not be revealed through analysis of single gene perturbations, single drug perturbations or single drug/gene combinations using either single cell or population level readout.

DISCUSSION

Here we use genetic interaction maps measured under reference and environmentally perturbed conditions to explore conditional genetic dependencies. To our knowledge, this study constitutes the first systematic measurement of genetic interactions under different environmental states in human cells and serves two key areas of inquiry into gene functional relationships. First, our maps are a resource for exploring the specific relationships between genes under basal conditions, upon perturbation of the S-phase checkpoint, upon exposure to exogenous genotoxic chemicals, and upon deprivation of glucose. Each map provides almost 50,000 unique gene-gene relationships and hierarchical clustering information that illuminates both known and unexpected features of this biology.

Second, our data are among the first systematic pieces of evidence to demonstrate simplistic models that imply a one gene, one function relationship are likely not sufficient to fully explain complex features of human cell biology and reveal the surprising degree to which gene relationships are plastic. We arrived at this conclusion because despite reproducible validation of the relationships between genes, and the conservation of clustering of functional groups in all maps, we find the overlap of specific interactions between maps to be strikingly small. This unexpected result suggests gene connections are rewired when cells are introduced to a different environment. Interestingly, rather than a diffuse distribution of rewired GIs, we observed that a relatively small number of genes and protein complexes are responsible for much of the rewiring GI signal. Namely in the context of S-phase checkpoint biology, we identify the TIP60 histone acetyltransferase complex as a driving force in the ATR

inhibited genetic landscape. TIP60 displays rewired GIs with many ontologies in the map, particularly those involved in cell cycle modulation, gene expression, and metabolism. Knockdown of TIP60 leads to large changes in gene expression and, critically, results in a transcriptional cell state that is seemingly epistatic to ATR inhibition.

It would be of interest in future studies to disambiguate the direct versus indirect effects that result from perturbation of the TIP60 complex in the context of impaired ATR signaling. The specific genes found to be transcriptionally downregulated upon perturbation of the TIP60 complex implicate some control over metabolic programs which is consistent with the slow growth phenotypes observed under baseline TIP60 knockdown conditions. TIP60 also forms condition specific and negative eGIs with a number of these key homeostatic factors (mitochondrial respiration, one-carbon metabolism, etc). Perhaps TIP60 is responsible for transcriptional control over several key homeostatic pathways, and its perturbation serves to generally slow the rate of energy production in the cell. This could prove protective against ATR inhibition, which is generally lethal to cells in its precipitation of mitotic catastrophe from premature entry to M-phase with incomplete replication or unrepaired damage to DNA (*44*).

The promise of genetic interaction mapping is understanding the full interdependence of every gene in the genome. With such a tool, a deep pool of knowledge can be pulled upon to inform hypotheses and comprehend how the vast circuitry of the cell collaborates to achieve homeostasis. The myriad environments faced by, and genetic variability inherent in, every organism requires an adaptability that cannot be captured with static gene networks. We show how a collection of genes

tasked with responding to an existential cellular threat, the loss of a critical checkpoint regulator, work in concert to help or hamper the cell's ability to maintain homeostasis and how these circuits shift dramatically in response to a changing environment.

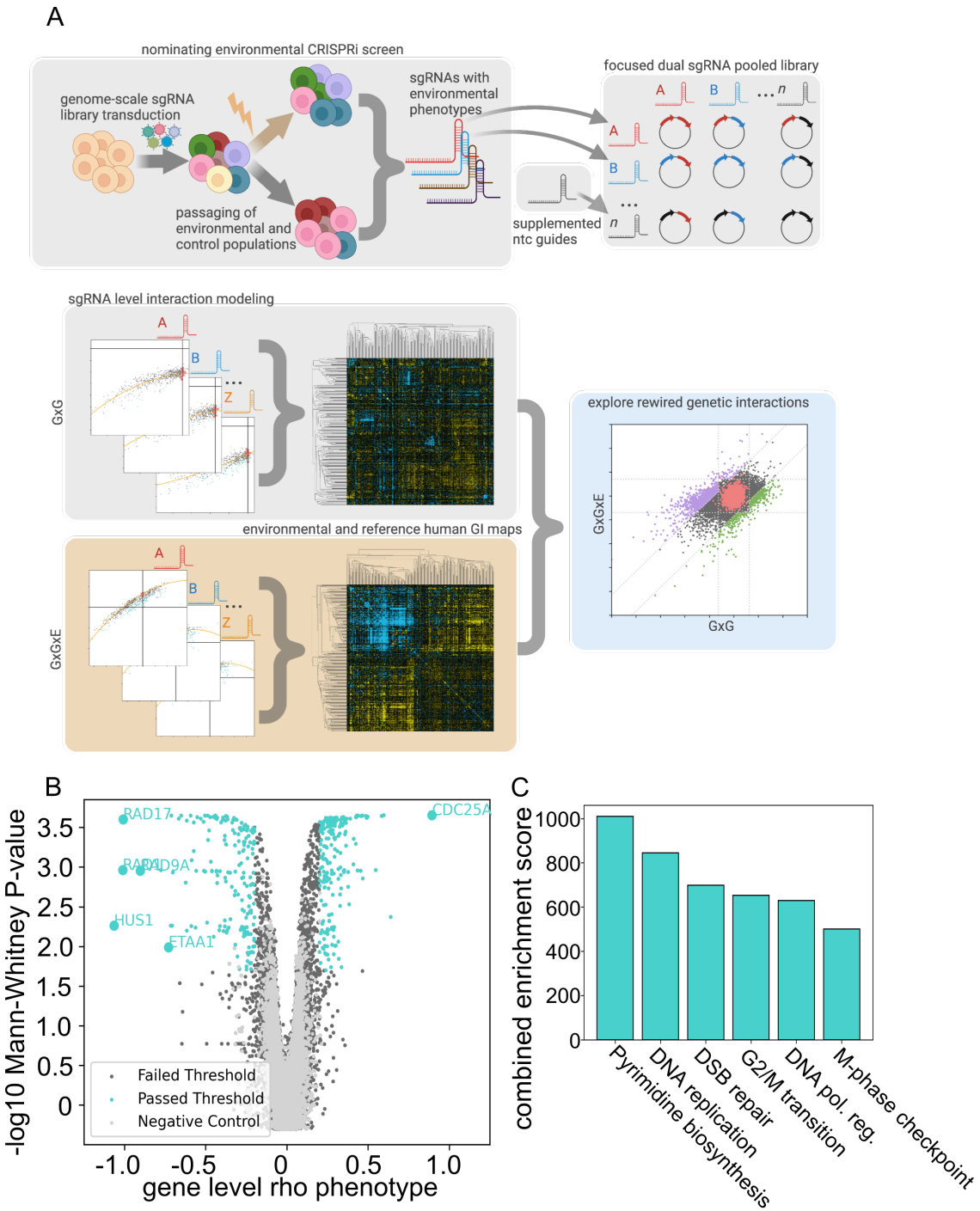

Figure 1: A high-fidelity CRISPRi screen for ATRi modulators.
A, Experimental workflow for exploring genetic rewiring in human cells. ATRi associated genes nominated from CRISPRi genome scale screens can be used to create conditional genetic interaction maps that allow for exploration of differential gene functional connections. **B**, Volcano plot of gene-level rho score (growth normalized drug perturbation phenotypes, see methods) and Mann-Whitney p-value results from

nominating K562 CRISPRi screen. All 293 threshold passed “hit” genes are highlighted in blue. **C**, Gene ontology term enrichment from the nominating screen hit list using the “combined score” metric from Enrichr.

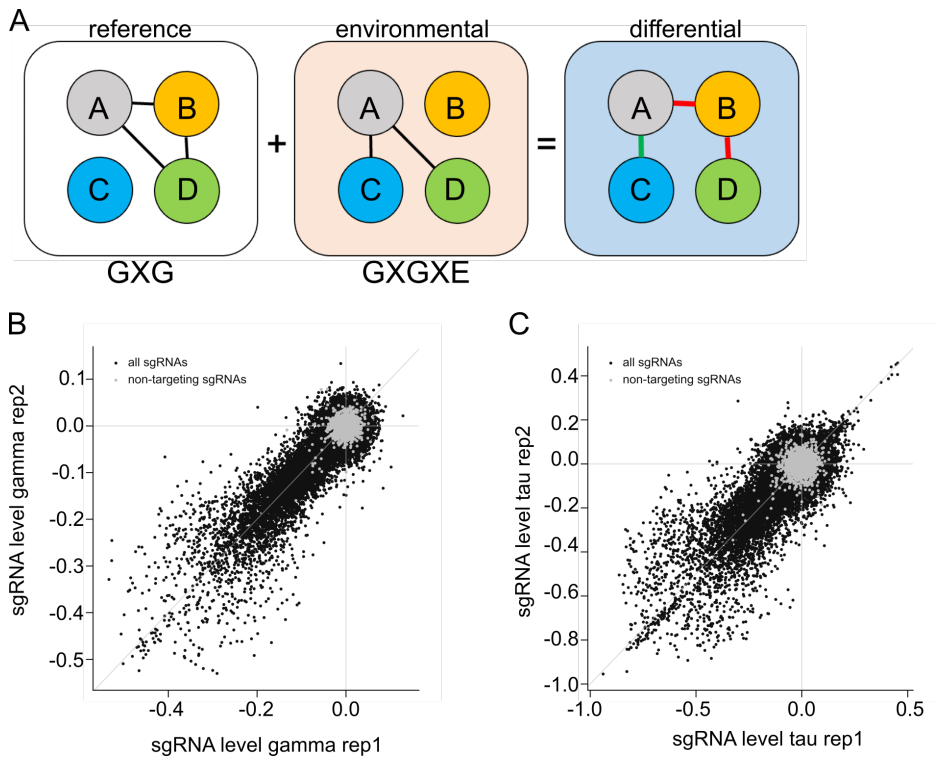

Figure 2: A framework for measuring rewired genetic interactions.
A, Cartoon example of genetic interaction rewiring across environmental conditions. **B**,**C** Scatterplots of sgRNA level phenotypes for the gamma scores from the untreated arm of the experiment (B) and the tau scores from the ATR inhibitor treated arm of the experiment (C) (see methods). Each individual gene targeting sgRNA shown in black. Non-targeting control guides shown in light gray.

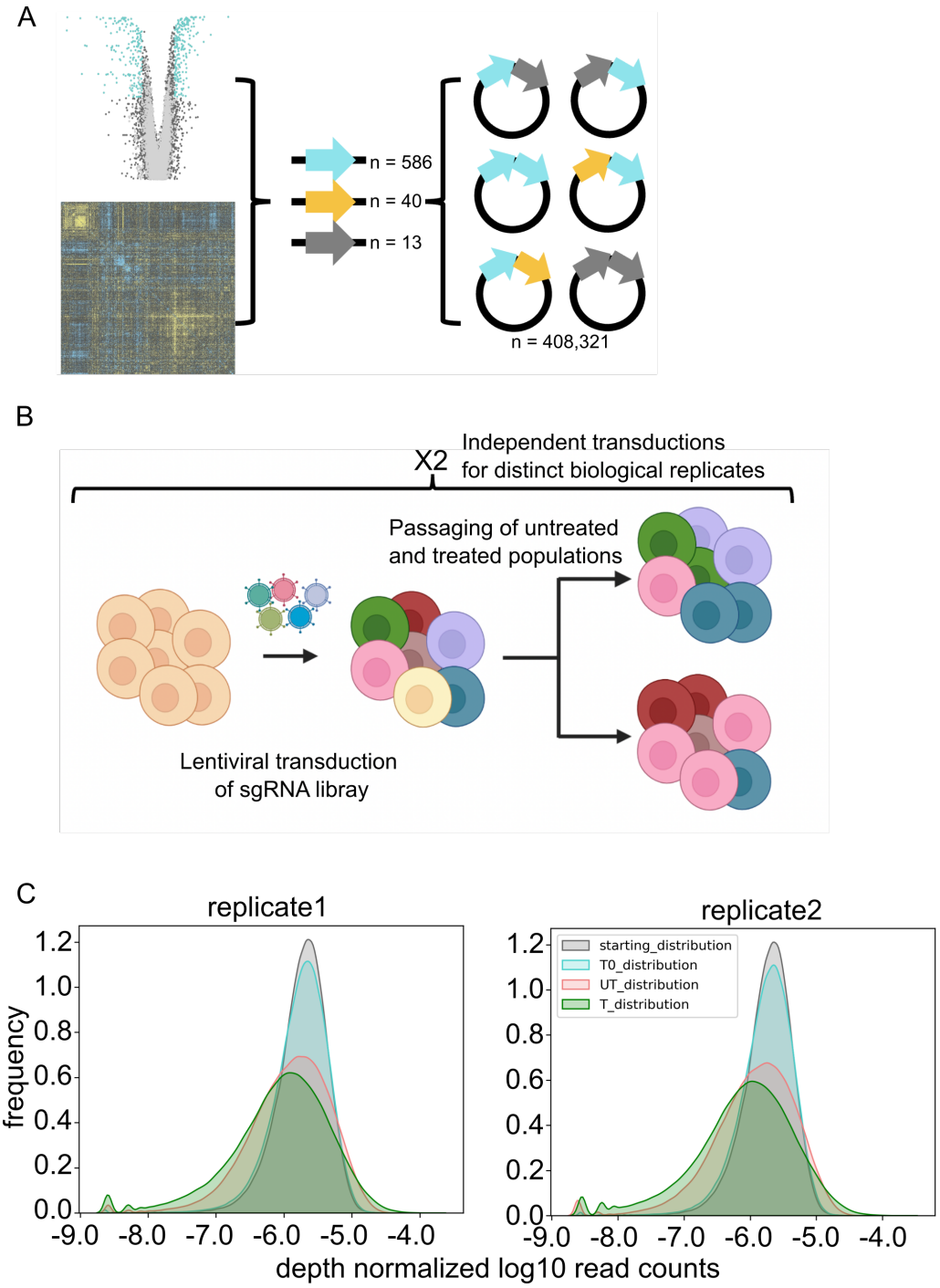

Figure 3: Schemes for nominating screen and pooled GI library cloning.
A, GI/eGI library design. Cyan arrows denote sgRNAs that induce an ATRi specific growth response validated from our nominating screen. Yellow arrows denote sgRNAs validated from previous studies that are relevant to DNA repair and cell cycle biology but not included from the nominating screen. Gray arrows denote non-targeting control sgRNAs picked from the nominating screen based on their lack of phenotype in either

condition (ATR inhibited or untreated). **B**, Overall strategy for both the nominating CRISPRi screen and GI/eGI screens in K562 cells (see methods for details). **C**, Kernel density plots of read counts mapped from our GI library for both independent replicates normalized by the sum of reads in each condition shown: pre-transduction, timepoint zero, final timepoint untreated, final timepoint ATRi treated (gray, blue, red, and green, respectively).

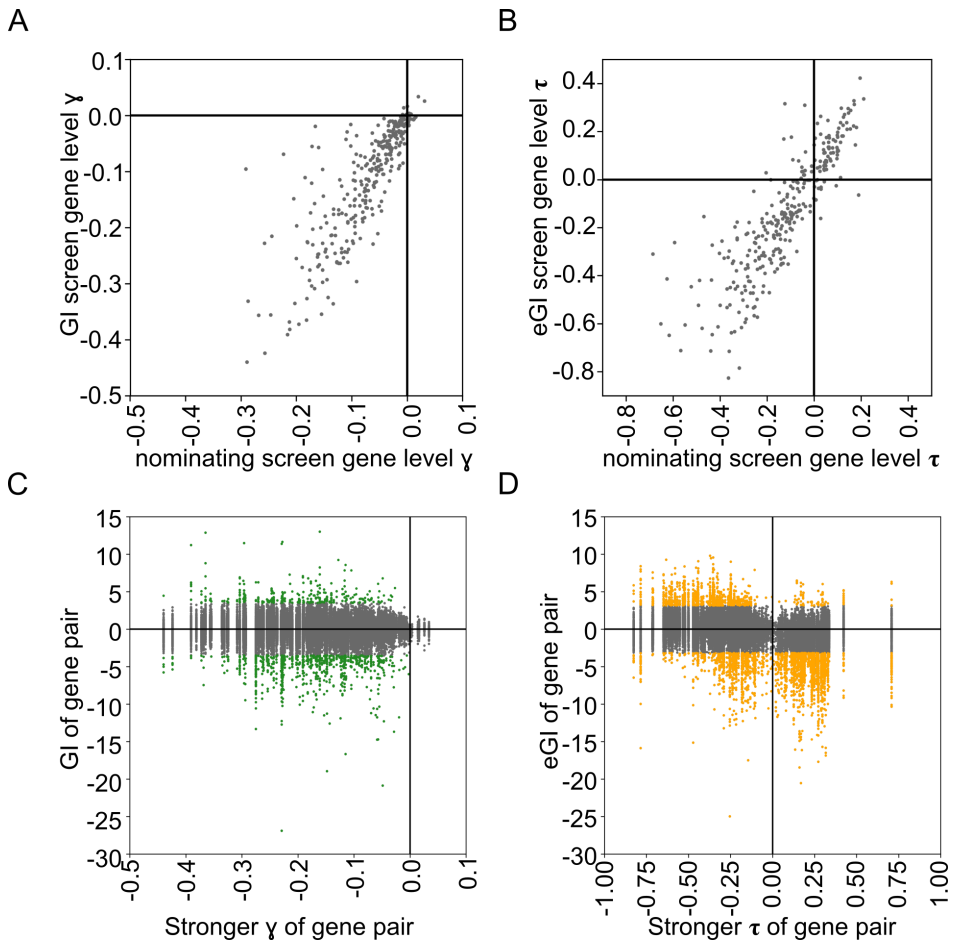

Figure 4: Quality control of GI and ATRi eGI datasets.
A,**B**, Scatterplots of the gene level untreated or ATRi treated phenotypes (gamma and tau, respectively) calculated in our nominating CRISPRi screen versus the same phenotypes calculated in our GI and eGI screens. **C**,**D**, Scatterplots of the stronger (farthest from zero) single guide gamma (C) or tau (D) score calculated for each pair of sgRNAs versus the GI or eGI calculated between that pair. Gene pairs with a significant GI or eGI score are highlighted in green and orange, respectively.

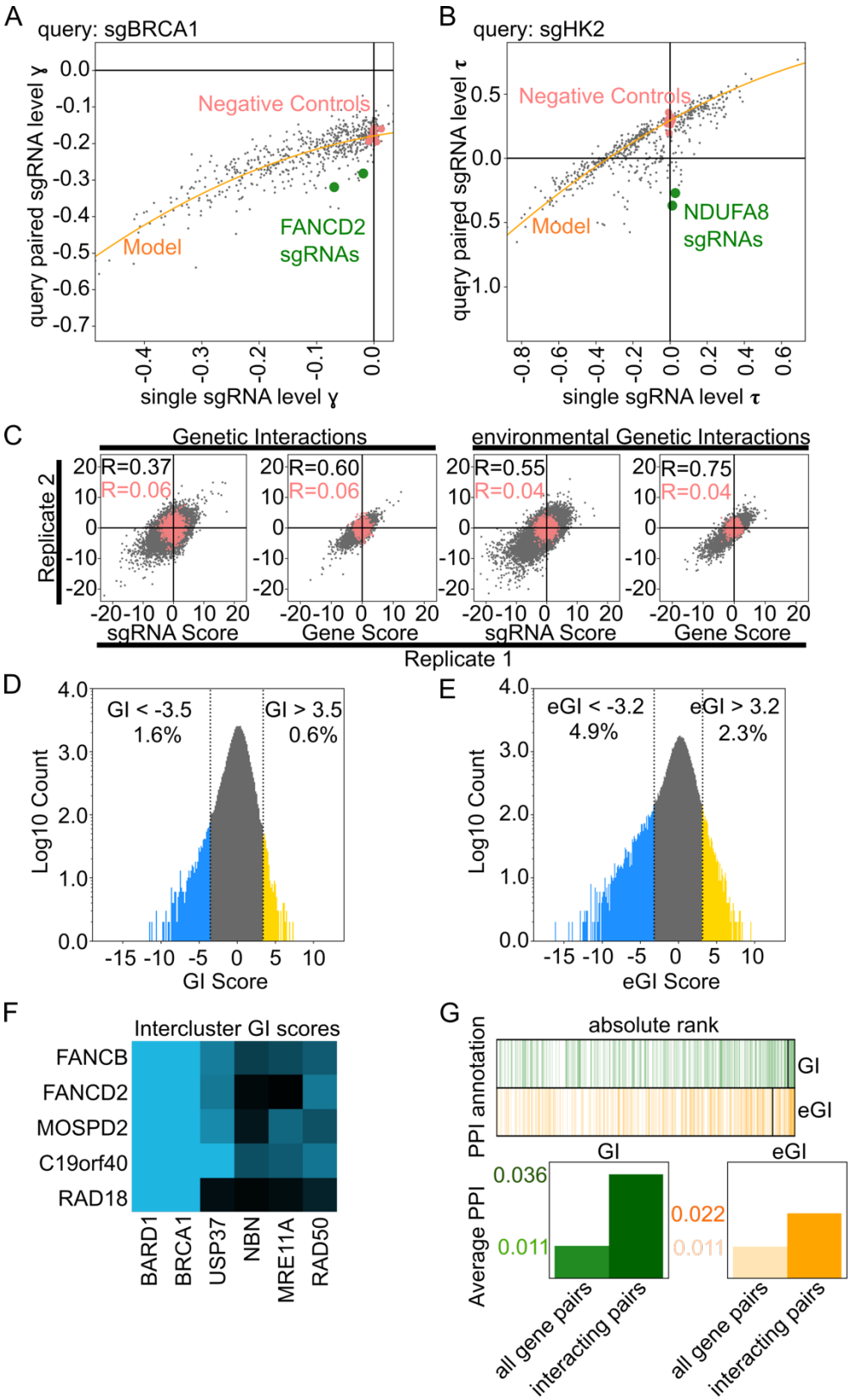
A
query: sgBRCA1
query paired sgRNA level γ
single sgRNA level γ
Negative Controls
Model
FANCD2
sgRNAs
B
query: sgHK2
query paired sgRNA level τ
single sgRNA level τ
Negative Controls
Model
NDUFA8
sgRNAs
C
Genetic Interactions
environmental Genetic Interactions
Replicate 2
Replicate 1
R=0.37
R=0.06
R=0.60
R=0.06
R=0.55
R=0.04
R=0.75
R=0.04
sgRNA Score
Gene Score
sgRNA Score
Gene Score
D
GI < -3.5
1.6%
GI > 3.5
0.6%
Log10 Count
GI Score
E
eGI < -3.2
4.9%
eGI > 3.2
2.3%
Log10 Count
eGI Score
F
Intercluster GI scores
FANCB
FANCD2
MOSPD2
C19orf40
RAD18
BARD1
BRCA1
USP37
NBN
MRE11A
RAD50
G
absolute rank
PPI annotation
GI
eGI
GI
eGI
Average PPI
0.036
0.011
0.022
0.011
all gene pairs
interacting pairs
all gene pairs
interacting pairs

Figure 5: Calling genetic interactions in variable conditions.
A,**B**, Example dual-sgRNA phenotype modeling and genetic interaction calling for *BRCA1* untreated (A) and *HK2* ATRi treated (B) query perturbations. Negative control distributions for the query sgRNA are highlighted in red. The model derived from regression of the distributions of single versus query paired sgRNAs is in orange. The two sgRNAs of an example positive control gene anticipated to interact with the query gene are highlighted in green. **C**, Correlation of sgRNA and gene-level genetic interactions between replicates in the untreated and ATRi treated conditions. The distributions of ntc paired sgRNA and gene level interactions are in red. For gene level plots, a circle is drawn centered on the origin with radius representing four times the standard deviation of the gene-ntc distribution. **D**,**E**, Distributions of genetic interaction scores called between all gene pairs for untreated (D) and treated (E) conditions. Significance thresholds are represented by vertical dotted lines. Negative and positive interactions beyond the threshold are highlighted in blue and yellow, respectively. **F**, Matrix of genetic interactions from the untreated map between genes annotated in the Fanconi Anemia complementation group and the *BRCA1*/*BARD1* and MRN complexes. Blue squares denote a negative interaction. **G**, (upper) Rug plot of the absolute value of all GI and ATRi eGI scores by ascending rank, annotated with PPI data from the STRING database. Black vertical lines indicate threshold values used to call significantly sized interactions. (lower) Average STRING PPI scores for all interactions considered not significant (lighter colors) and significant (darker colors).

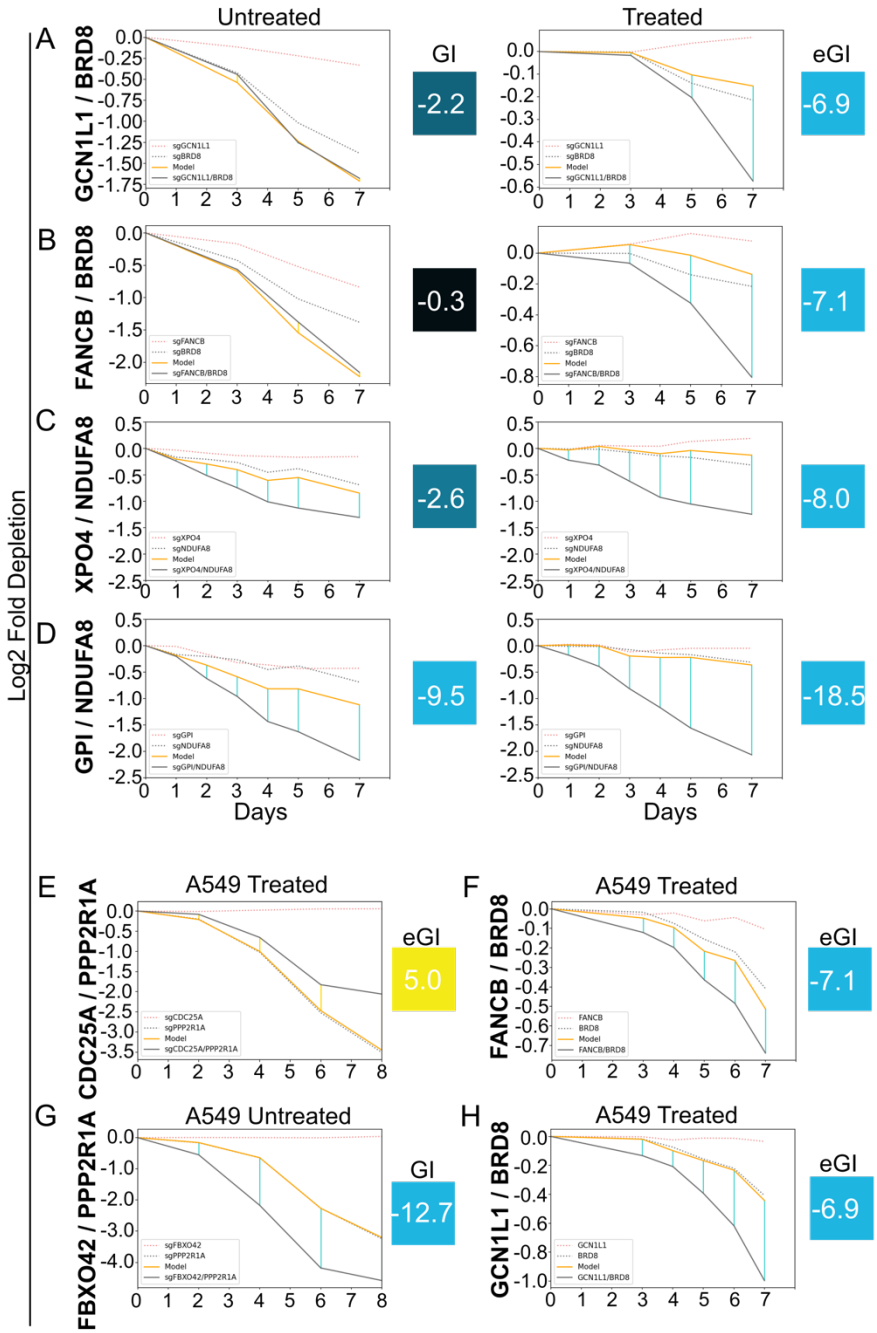

Figure 6: Fluorescence competition assays validate putative interactions. **A-D**, Assays to validate environmental conditionality of interactions. Depletion phenotypes of single gene perturbations over time are shown as dotted lines. Modeled paired phenotypes are shown as orange solid lines. Observed paired phenotypes are shown as gray solid lines. Interaction scores are shown as vertical lines between modeled and observed paired phenotypes at all timepoints measured, either blue or yellow to denote a negative or positive interaction, respectively (see methods). The GI and ATRi eGI scores shown to the right of the plots are the observed interactions from our maps. **E-H**, Assays to validate interactions in A549 cells. Plot structure is the same as in Fig. 6A-D.

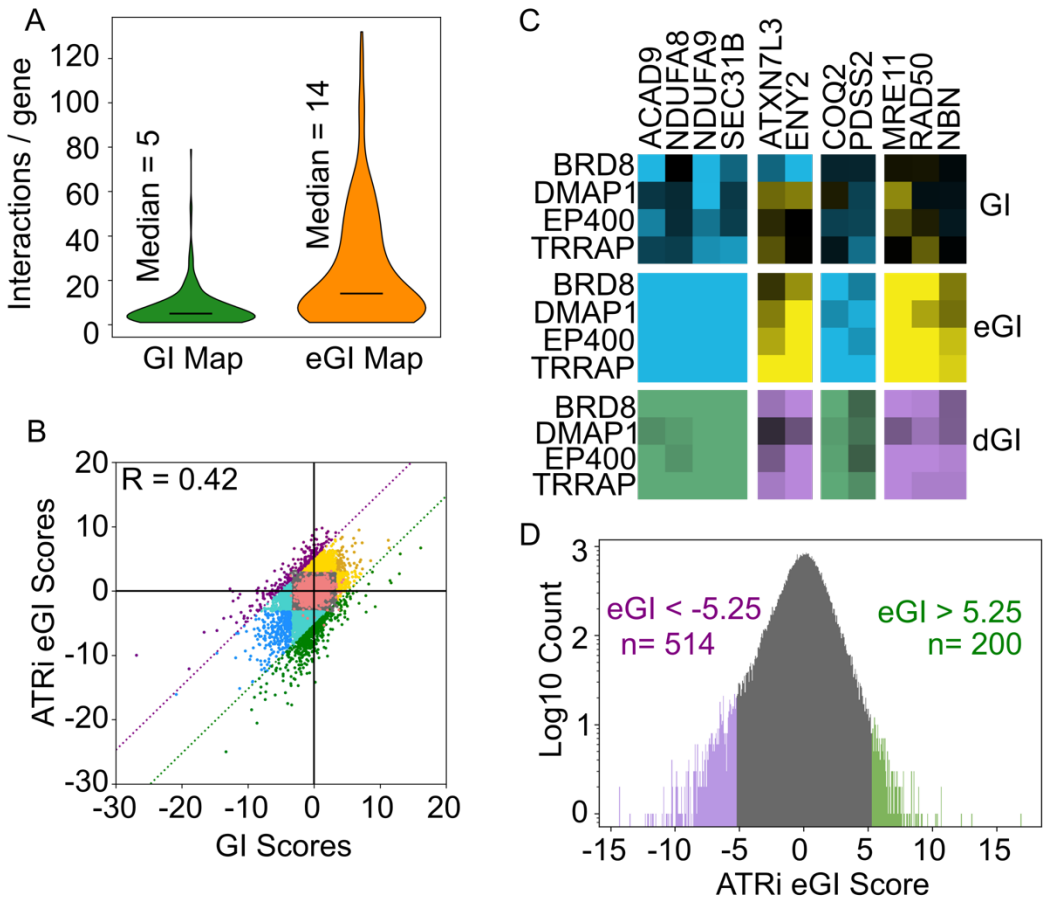

Figure 7: Analysis of condition specific genetic interaction in response to ATRi. **A**, Violin plot of the distribution of the number of genetic interactions found for each gene in both the GI and ATRi eGI maps. **B**, Scatter plots of all gene pair genetic interactions and ATRi environmental genetic interactions. Significance thresholds for dGIs are denoted by dotted diagonal lines. Gene pairs with a negative or positive interaction specific to either map are highlighted in light blue or light yellow, respectively. Gene pairs with a negative or positive interaction in both maps are highlighted in dark blue, or dark yellow, respectively. **C**, Example of genetic interaction rewiring between various clusters of genes. **D**, Distribution of dGI scores with significance thresholds for negative and positive differential interactions highlighted in purple and green, respectively.

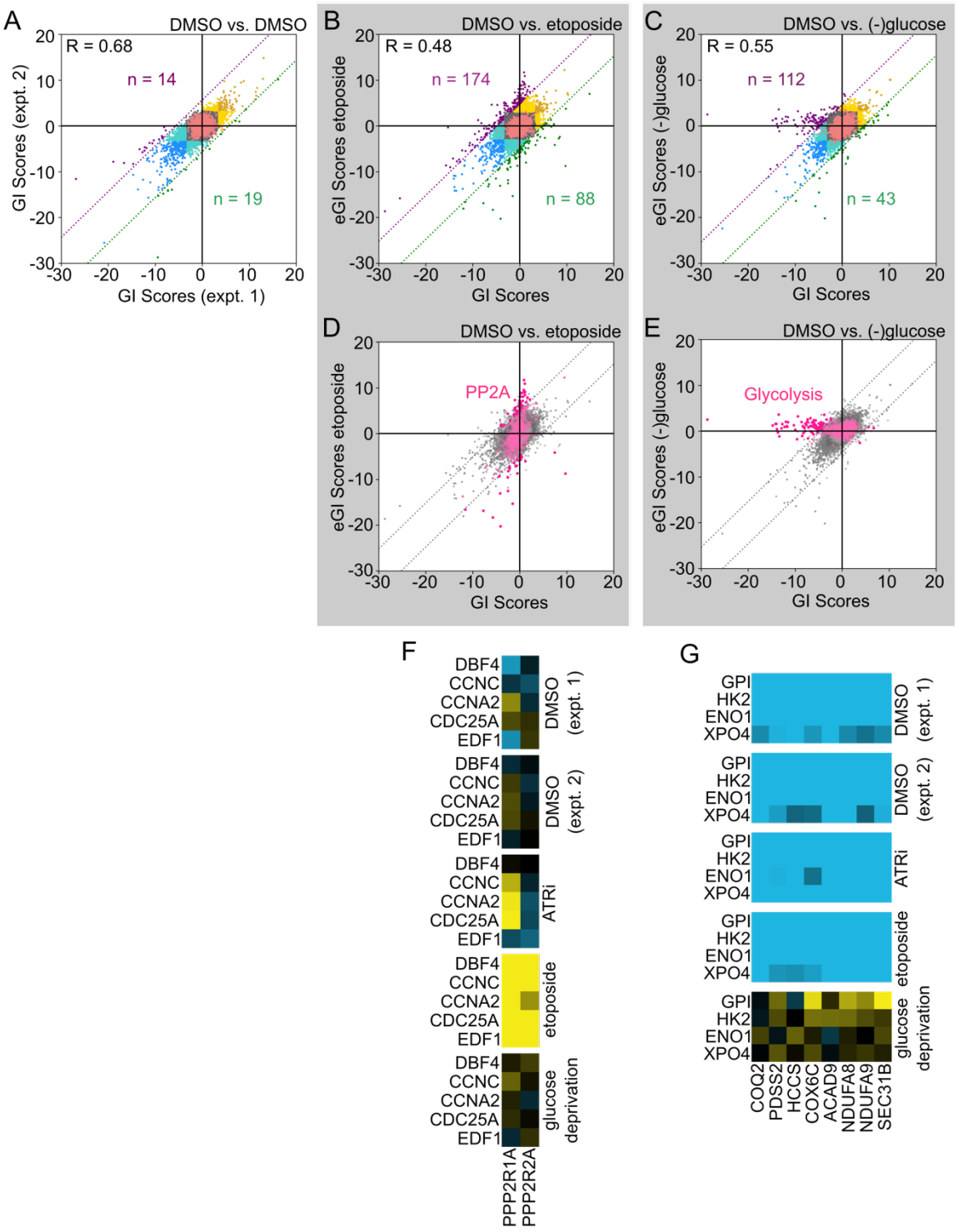

Figure 8: Genotoxic and glucose deprived environments produce a unique set of rewired genetic interactions.

A, Scatterplot of GI scores measured in the reference (untreated/DMSO) map from the initial round of experiments versus the same scores in the second set of experiments.

Color scheme is the same as Fig. 7B. **B, C,** Scatterplots of GI/eGIs measured in the second set of experiments between the etoposide or glucose deprived condition and the matched reference map. Color scheme is the same as Fig. 7B. **D, E,** The same scatterplots as shown in 8B,C but with gene pairs that contain a gene implicated in a ontology that drives the rewiring signal highlighted in pink. dGI threshold passed interactions are further bolded. **F, G,** Individual genetic interactions shown for a set of genes that drive the rewiring signature in the etoposide or glucose deprived map against an example set of ontologically consistent genes for all five GI and eGI maps.

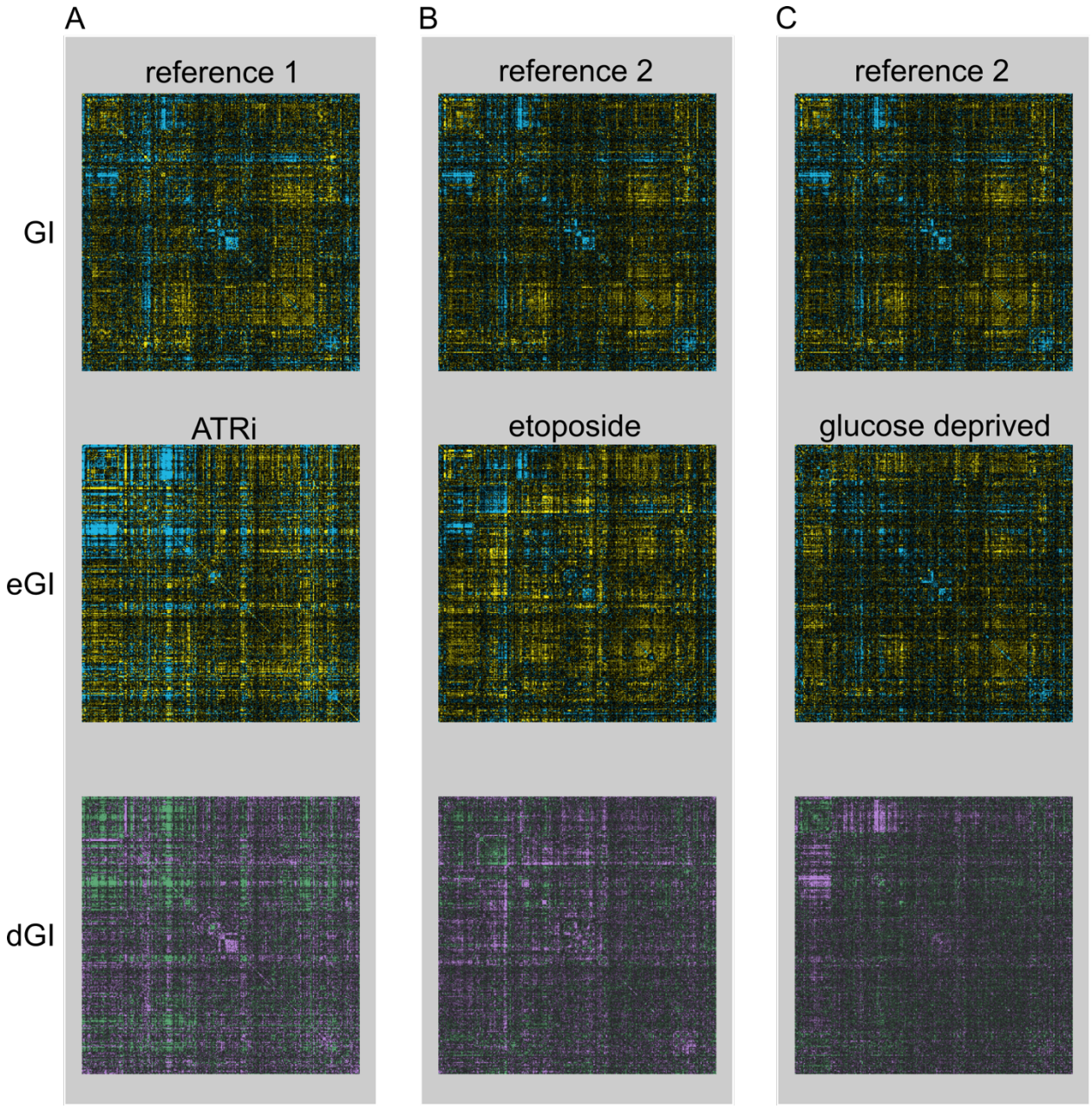

Figure 9: Clustered GI, eGI, and dGI matrices for all reference and environmental conditions.
A-C, Heatmaps of GI, eGI, and dGI scores for each reference and environmental condition clustered using the consensus of each genes normalized interaction profile across all maps. In GI and eGI maps, blue and yellow indicate negative and positive interactions, respectively. Difference maps for the ATRi (A), etoposide treated (B), and glucose deprived (C) conditions are illustrated using negative and positive differential interactions in green and purple, respectively.

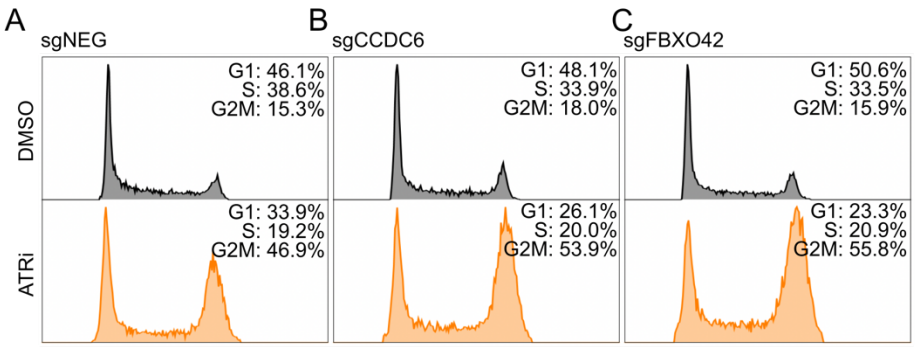

Figure 10: Influence on cell cycle distribution of CCDC6/FBXO42 knockdown. **A-C**, Propidium iodide staining for DNA context of dividing cells expressing a non-targeting guide (A), a guide targeting *CCDC6* (B) or a guide targeting *FBXO42* (**c**) under basal (DMSO) or ATR inhibited conditions.

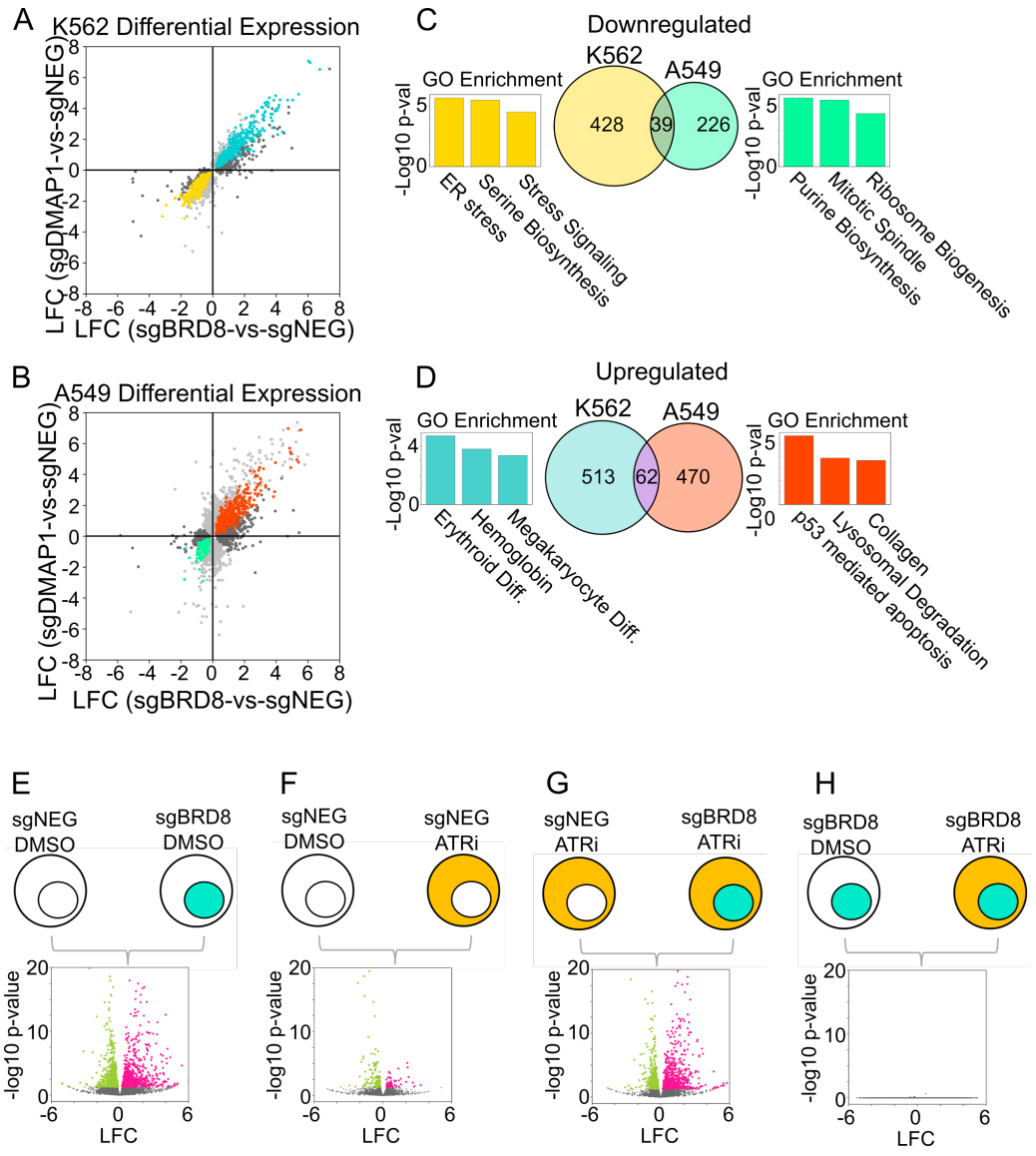

Figure 11: Analysis of the effects of TIP60 knockdown on gene expression and DDR activity.

A, B, Scatterplot of log fold change (LFC) in gene expression in K562 or A549 cells upon perturbation of either BRD8 or DMAP1 relative to non-targeting control (sgNEG). Genes in dark gray and light gray are found to be significantly (adjusted p-value < 0.05) differentially expressed specifically in the *BRD8* or *DMAP1* perturbations, respectively. Colored genes are significantly differentially expressed in both perturbations. **C**, **D**, Venn-Diagrams of overlap in differentially expressed genes that are regulated by both *BRD8* and *DMAP1* perturbation between cell types. Gene-ontology term enrichment derived from each grouping of genes by Enrichr. **E-H**, Volcano plots of four differential expression comparisons in K562 cells upon perturbation of *BRD8*, treatment with ATRi or both.

METHODS

Experimental Materials & Methods

Mammalian cell line culture and lentivirus preparation

All mammalian cell lines were cultured at 37˚C with 5% CO2. K562 cells stably expressing dCas9-KRAB were grown in RPMI-1640 media with 25mM HEPES (GIBCO), supplemented with 10% FBS, 100units/mL Penicillin, 100µg/mL Streptomycin, and 292µg/mL Glutamine (GIBCO). During the nominating and GI screens, K562 were grown in shaker flasks in a dedicated cell culture shaker/incubator (INORS) at 120rpm and the media these cells were grown in was further supplemented with 0.1% Pluronic surfactant (GIBCO). A549 cells stably expressing dCas9-KRAB were grown in F12K media supplemented with 10% FBS, 100units/mL Penicillin, 100µg/mL Streptomycin, 292µg/mL Glutamine (GIBCO), 1x MEM Non-Essential amino acids (GIBCO), and 1mM Sodium Pyruvate (GIBCO). HEK293T cells were grown in DMEM media supplemented with 4.5g/L D-Glucose, 110mg/L Sodium Pyruvate (GIBCO), 10% FBS, 100units/mL Penicillin, 100µg/mL Streptomycin, 292µg/mL Glutamine (GIBCO). Lentivirus was prepared from HEK293T cells using TransIT-LT1 transfection reagent (MIRUS) and standard three-vector packaging plasmids. 72hr post-transfection, viral supernatant is filtered with 0.45µm filters and frozen at -80˚C.

sgRNA expression vector and library design

All sgRNAs used in all experiments were derived from a previously described list of the top5 algorithmically determined CRISPRi guides for each protein-coding gene in the genome. This genome-scale CRISPRi library was used for the nominating CRISPRi ATRi screen.

To clone the library used for GI mapping: the two sgRNAs with the strongest phenotype from each of the 293 genes in the nominating screen with a $|\boldsymbol{\rho}|$ score (see below) of >0.2 and $-\log_{10}$ Mann-Whitney p-value >2.0 were used as the basis for our focused GI library. To this list of 586 sgRNAs, 40 more were included targeting 20 genes with a known connection to a range of gene ontologies pertaining to the DNA damage response that had been validated in a previous project. Finally, 13 negative control sgRNAs were included bringing the total size of the library to 639 unique sgRNAs (Extended Data Fig. 2b, Supplementary Table 2). Protospacers for this library were obtained in a pooled format commercially, subsequently cloned into two independent intermediate vectors, then cloned into the final dual sgRNA expression vector in which every possible pairwise permutation of sgRNAs in the singles library is represented, as described previously. Through attrition inherent in cloning large sgRNA libraries, a small percentage (<1%) of sgRNA pairs were lost, resulting in a realized library size of 405,667 with 90% of all elements expressed at <16-fold variation.

Dual sgRNA vectors used in fluorescence competition validation experiments were cloned in the same expression vector as used in the GI library, in an arrayed format.

Single sgRNA vectors used in RNAseq experiments were cloned into the same vector used in the nominating CRISPRi screen, in an arrayed format.

Transduction and screening with CRISPRi libraries

Transduction and passaging of cells are done in duplicate as independent biological replicates for all experiments. For both the nominating and GI screens, K562 cells stably expressing dCas9-KRAB were transduced with a lentiviral preparation of an sgRNA library using 8μg/mL polybrene with the goal of obtaining a transduced population representing at least 250-fold coverage of the library while maintaining an MOI below 0.3. This population of cells is grown and expanded continuously and dosed with puromycin at a concentration of 1μg/mL 48 and 72 hours post transduction to select for infected cells. The infected population is expanded until at least 4000-fold coverage of infected cells are available to begin the screen. At the initial time point, cell pellets with 1000-fold coverage of the library are frozen in 10% DMSO freezing media. This initial timepoint was taken at day six and day seven post transduction for the nominating screen and GI screens respectively.

For the nominating screen, samples are split to a concentration of 2.5e5 cells/mL every other day in fresh media. On days zero and seven of the screen the treated sample is dosed with 750nM AZD6738, and the untreated samples are dosed with an equivalent volume of DMSO. Fifteen days after the start of the experiment, once the cumulative difference in population doublings between the treated and untreated samples had approximately reached five, the final time point was taken; 1000-fold coverage worth of cells were frozen down in each condition, as before.

For GI screening, samples are split every day to a concentration of 5e5 cell/mL in fresh media. On days zero and seven of the screen, the treated sample is dosed with 1.25μM AZD6738, and the untreated samples are dosed with an equivalent volume of DMSO. Final timepoint samples were frozen down on day nine after the cumulative difference in population doublings between the treated and untreated populations exceeded 4.5 in both replicates.

For both nominating and GI screens, genomic DNA was extracted from T0 and final timepoint cell pellets using a Macherey-Nagel Blood XL cleanup kit. Integrated sgRNA loci were amplified from gDNA using PCR to append adapters for NGS, then submitted for sequencing on an Illumina Hiseq4000 or NovaSeq platform, for the nominating and GI screens respectively. For GI libraries, a hamming distance of one is used when mapping reads to our reference library, to allow for minor errors in sequencing to not be excluded from analysis. Custom sequencing primers were used for both nominating screen and GI maps as described previously.

Fluorescence competition assays

K562 or A549 cells are transduced with a lentiviral preparation of a single or dual sgRNA expression vector and expanded continuously for several days. At day five post transduction, cells are seeded at a concentration of 5.0e5 cells/mL and dosed with 1.25μM AZD6738 or an equivalent volume of DMSO, constituting the d0 sample. Each condition is analyzed by flow cytometry everyday or every other day to determine the ratio of uninfected control cells to BFP+ transduced experimental cells before being reseeded at 5.0e5 cells/mL in fresh medium. This process is repeated until seven or

eight days after the first dose or the transduced population falls below 1% of the total population.

Data is processed by normalizing all samples by their day 0 %BFP+ to calculate the deviation from the starting value. To account for random variation in data collection, each timepoint for each sample is then further normalized by the deviation observed in the ntc/ntc dual sgRNA sample at that same timepoint. The log2 of these values is taken to derive the enrichment/depletion phenotype. Next, a matrix of modeled dual sgRNA phenotypes is calculated by summing the phenotypes from samples with only a single targeting sgRNA at each timepoint. The difference between phenotypes from the observed dual sgRNA vectors and the modeled phenotype derived from the single sgRNA vectors is recorded as the validation genetic interaction.

Propidium Iodide (PI) Staining of DNA content

Pure populations of cells transduced with an sgRNA targeting *CCDC6*, *FBXO42*, or ntc were grown in media treated with 1.2μM AZD6737 or an equivalent volume of DMSO for 24hr. Cells were washed and grown in fresh untreated media for another 24hr before harvesting for PI staining (total time post treatment = 48hr). To prepare for staining and flow cytometry, cells were washed in PBS (GIBCO) and cell pellets resuspended in ice-cold 70% EtOH while being vortexed. Fixation continued at -20˚C for 1hr, then cells were washed in PBS and analyzed by flow cytometry to determine concentration. 5E5 fixed cells were spun down and resuspended in 500μL of PI/RNase staining solution (Invitrogen). Cells were stained for 30minutes then analyzed by flow cytometry to determine DNA content distributions of each population.

RNAseq

K562 cells are transduced with a lentiviral preparation of a single sgRNA expression vector targeting either *BRD8*, *DMAP1*, or ntc in replicate. 48hr post-transduction cell populations are sorted by %BFP+ to obtain a pure population of transduced cells and expanded continuously for several days. On day five post-transduction, cell populations are dosed with 1.5μM AZD6738 or an equivalent volume of DMSO. 48hr hours after dosing 1.0e6 cells are harvested from each sample. RNA is then extracted from cell pellets using a Zymo Direct-Zol kit. 350ng of RNA from each sample is used as the input for the Lexogen Quantseq FWD kit with UMI add-on. All steps of the kit are performed according to the manufacturer's instructions.

Analytic Methods

Calculating sgRNA level growth phenotypes from CRISPRi screens

Calculating primary sgRNA level growth phenotypes from raw sequencing counts data for both the nominating CRISPRi and GI screens were done in the same way. First, each sgRNA construct within a sample is normalized by the total read counts for all sgRNAs in that sample, to adjust for differences in sequencing depth. Phenotypes in an untreated condition (**γ**), or treated condition (**τ**) are calculated as:

$$\gamma = log_2\left(\frac{R_F/N_F}{R_0/N_0}\right) * \frac{1}{d_u}$$

$$\tau = log_2\left(\frac{R_T/N_T}{R_0/N_0}\right) * \frac{1}{d_t}$$

where $\mathbf{R_F}$, $\mathbf{R_T}$, and $\mathbf{R_0}$ are the number of reads for the query sgRNA construct in the final untreated, final treated, and initial time points respectively. $\mathbf{N_F}$, $\mathbf{N_T}$, and $\mathbf{N_0}$ are

the median number of reads among negative controls (negative-negative pairs in GI screens) in the final untreated, final treated, and initial timepoints, respectively. $\mathbf{d_u}$ and $\mathbf{d_t}$ are the cumulative number of cell population doublings in the experiment in the untreated and treated conditions, respectively.

Additionally, to calculate the guide normalized effect on cell viability in the treated condition, that is used to threshold hits in the nominating screen (**ρ**), we use:

$$\rho = log_2\left(\frac{R_T/N_T}{R_F/N_F}\right) * \frac{1}{d_u - d_t}$$

In the GI screen, sgRNAs with median read counts less than 35 in either orientation (either first or second) in the expression vector in any condition are removed from analysis in all conditions. Additionally, a pseudocount of 10 is added to each sgRNA's read count that passes this threshold. Single sgRNA level phenotypes are then determined by averaging the **γ** or **τ** of each sgRNA paired with all thirteen negative controls in both orientations (26 independent measurements per sgRNA, 52 per gene).

Calculating genetic interactions

A GI model is generated for each single query sgRNA by quadratic regression of the relationship between all single sgRNA phenotypes and every paired sgRNA phenotype in which the query sgRNA is present (Fig. 2a). A genetic interaction for all query paired sgRNA constructs is then calculated based on the deviation of that pair's phenotype from the model. These differences are then z-score normalized by the standard deviation of the negative control distribution for that guide (standard deviation of phenotypes in the population of 26 query sgRNA-ntc pairs). GIs called for each unique pair of sgRNA are averaged across both orientations of that pair (first and

second in the construct). Gene level GIs are called by averaging all four orientations of guides that target those genes.

GO term enrichment

The enrichr function of the gseapy module in python was used to determine GO term enrichment of gene sets from the nominating ATRi screen, GI/eGI maps, and RNAseq datasets. The gene sets used as a reference were "GO_Biological_Process_2021" and "GO_Molecular_Function_2021". GO terms were considered significantly enriched in a gene set if the -log10 adjusted p-value associated with the term was >=6.

Clustering genes by GI profile

GI and eGI matrices were clustered using the "clustermap" function of the seaborn package in python with the "method" and "metric" variables assigned as "average" and "correlation" respectively. A consensus clustering was created by normalizing each map by its population level variation, then concatenating all maps together to form a n by 5*n element matrix from which the finalized clustering was derived.

Differential expression analysis of RNAseq data

Differential expression of genes calculated from RNAseq data was analyzed using the DeSeq2 package in R. Genes with fewer than 10 reads across all replicates and conditions were removed from the analysis as they are assumed to not be

expressed in either K562 or A549 cells. All comparisons between conditions within a cell line were used to generate differential expression log-fold change and associated p-values.

REFERENCES

1. A. Tsherniak, F. Vazquez, P. G. Montgomery, B. A. Weir, G. Kryukov, G. S. Cowley, S. Gill, W. F. Harrington, S. Pantel, J. M. Krill-Burger, R. M. Meyers, L. Ali, A. Goodale, Y. Lee, G. Jiang, J. Hsiao, W. F. J. Gerath, S. Howell, E. Merkel, M. Ghandi, L. A. Garraway, D. E. Root, T. R. Golub, J. S. Boehm, W. C. Hahn, Defining a Cancer Dependency Map. *Cell*. **170**, 564-576.e16 (2017).
2. J. Barretina, G. Caponigro, N. Stransky, K. Venkatesan, A. A. Margolin, S. Kim, C. J. Wilson, J. Lehár, G. V. Kryukov, D. Sonkin, A. Reddy, M. Liu, L. Murray, M. F. Berger, J. E. Monahan, P. Morais, J. Meltzer, A. Korejwa, J. Jané-Valbuena, F. A. Mapa, J. Thibault, E. Bric-Furlong, P. Raman, A. Shipway, I. H. Engels, J. Cheng, G. K. Yu, J. Yu, P. Aspesi, M. de Silva, K. Jagtap, M. D. Jones, L. Wang, C. Hatton, E. Palescandolo, S. Gupta, S. Mahan, C. Sougnez, R. C. Onofrio, T. Liefeld, L. MacConaill, W. Winckler, M. Reich, N. Li, J. P. Mesirov, S. B. Gabriel, G. Getz, K. Ardlie, V. Chan, V. E. Myer, B. L. Weber, J. Porter, M. Warmuth, P. Finan, J. L. Harris, M. Meyerson, T. R. Golub, M. P. Morrissey, W. R. Sellers, R. Schlegel, L. A. Garraway, The Cancer Cell Line Encyclopedia enables predictive modelling of anticancer drug sensitivity. *Nature*. **483**, 603–607 (2012).
3. J. M. Replogle, R. A. Saunders, A. N. Pogson, J. A. Hussmann, A. Lenail, A. Guna, L. Mascibroda, E. J. Wagner, K. Adelman, G. Lithwick-Yanai, N. Iremadze, F. Oberstrass, D. Lipson, J. L. Bonnar, M. Jost, T. M. Norman, J. S. Weissman, Mapping information-rich genotype-phenotype landscapes with genome-scale Perturb-seq. *Cell*. **185**, 2559-2575.e28 (2022).
4. C. Stark, B.-J. Breitkreutz, T. Reguly, L. Boucher, A. Breitkreutz, M. Tyers,

BioGRID: a general repository for interaction datasets. *Nucleic Acids Res.* **34**, D535-539 (2006).

5. C. Boone, H. Bussey, B. J. Andrews, Exploring genetic interactions and networks with yeast. *Nat. Rev. Genet.* **8**, 437–449 (2007).
6. M. Costanzo, B. VanderSluis, E. N. Koch, A. Baryshnikova, C. Pons, G. Tan, W. Wang, M. Usaj, J. Hanchard, S. D. Lee, V. Pelechano, E. B. Styles, M. Billmann, J. van Leeuwen, N. van Dyk, Z.-Y. Lin, E. Kuzmin, J. Nelson, J. S. Piotrowski, T. Srikumar, S. Bahr, Y. Chen, R. Deshpande, C. F. Kurat, S. C. Li, Z. Li, M. M. Usaj, H. Okada, N. Pascoe, B.-J. San Luis, S. Sharifpoor, E. Shuteriqi, S. W. Simpkins, J. Snider, H. G. Suresh, Y. Tan, H. Zhu, N. Malod-Dognin, V. Janjic, N. Przulj, O. G. Troyanskaya, I. Stagljar, T. Xia, Y. Ohya, A.-C. Gingras, B. Raught, M. Boutros, L. M. Steinmetz, C. L. Moore, A. P. Rosebrock, A. A. Caudy, C. L. Myers, B. Andrews, C. Boone, A global genetic interaction network maps a wiring diagram of cellular function. *Science*. **353**, aaf1420 (2016).
7. M. Costanzo, G. Giaever, C. Nislow, B. Andrews, Experimental approaches to identify genetic networks. *Curr. Opin. Biotechnol.* **17**, 472–480 (2006).
8. S. J. Dixon, M. Costanzo, A. Baryshnikova, B. Andrews, C. Boone, Systematic mapping of genetic interaction networks. *Annu. Rev. Genet.* **43**, 601–625 (2009).
9. J. Domingo, P. Baeza-Centurion, B. Lehner, The Causes and Consequences of Genetic Interactions (Epistasis). *Annu. Rev. Genomics Hum. Genet.* **20**, 433–460 (2019).
10. S. R. Collins, K. M. Miller, N. L. Maas, A. Roguev, J. Fillingham, C. S. Chu, M. Schuldiner, M. Gebbia, J. Recht, M. Shales, H. Ding, H. Xu, J. Han, K.

Ingvarsdottir, B. Cheng, B. Andrews, C. Boone, S. L. Berger, P. Hieter, Z. Zhang, G. W. Brown, C. J. Ingles, A. Emili, C. D. Allis, D. P. Toczyski, J. S. Weissman, J. F. Greenblatt, N. J. Krogan, Functional dissection of protein complexes involved in yeast chromosome biology using a genetic interaction map. *Nature*. **446**, 806–810 (2007).

11. M. Costanzo, A. Baryshnikova, J. Bellay, Y. Kim, E. D. Spear, C. S. Sevier, H. Ding, J. L. Y. Koh, K. Toufighi, S. Mostafavi, J. Prinz, R. P. St Onge, B. VanderSluis, T. Makhnevych, F. J. Vizeacoumar, S. Alizadeh, S. Bahr, R. L. Brost, Y. Chen, M. Cokol, R. Deshpande, Z. Li, Z.-Y. Lin, W. Liang, M. Marback, J. Paw, B.-J. San Luis, E. Shuteriqi, A. H. Y. Tong, N. van Dyk, I. M. Wallace, J. A. Whitney, M. T. Weirauch, G. Zhong, H. Zhu, W. A. Houry, M. Brudno, S. Ragibizadeh, B. Papp, C. Pál, F. P. Roth, G. Giaever, C. Nislow, O. G. Troyanskaya, H. Bussey, G. D. Bader, A.-C. Gingras, Q. D. Morris, P. M. Kim, C. A. Kaiser, C. L. Myers, B. J. Andrews, C. Boone, The genetic landscape of a cell. *Science*. **327**, 425–431 (2010).
12. B. Fischer, T. Sandmann, T. Horn, M. Billmann, V. Chaudhary, W. Huber, M. Boutros, A map of directional genetic interactions in a metazoan cell. *eLife*. **4** (2015), doi:10.7554/eLife.05464.
13. J. A. Doudna, E. Charpentier, Genome editing. The new frontier of genome engineering with CRISPR-Cas9. *Science*. **346**, 1258096 (2014).
14. O. Shalem, N. E. Sanjana, E. Hartenian, X. Shi, D. A. Scott, T. Mikkelson, D. Heckl, B. L. Ebert, D. E. Root, J. G. Doench, F. Zhang, Genome-scale CRISPR-Cas9 knockout screening in human cells. *Science*. **343**, 84–87 (2014).

15. M. Nakamura, Y. Gao, A. A. Dominguez, L. S. Qi, CRISPR technologies for precise epigenome editing. *Nat. Cell Biol.* **23**, 11–22 (2021).
16. A. Pickar-Oliver, C. A. Gersbach, The next generation of CRISPR-Cas technologies and applications. *Nat. Rev. Mol. Cell Biol.* **20**, 490–507 (2019).
17. L. A. Gilbert, M. H. Larson, L. Morsut, Z. Liu, G. A. Brar, S. E. Torres, N. Stern-Ginossar, O. Brandman, E. H. Whitehead, J. A. Doudna, W. A. Lim, J. S. Weissman, L. S. Qi, CRISPR-mediated modular RNA-guided regulation of transcription in eukaryotes. *Cell*. **154**, 442–451 (2013).
18. D. Du, A. Roguev, D. E. Gordon, M. Chen, S.-H. Chen, M. Shales, J. P. Shen, T. Ideker, P. Mali, L. S. Qi, N. J. Krogan, Genetic interaction mapping in mammalian cells using CRISPR interference. *Nat. Methods*. **14**, 577–580 (2017).
19. M. A. Horlbeck, A. Xu, M. Wang, N. K. Bennett, C. Y. Park, D. Bogdanoff, B. Adamson, E. D. Chow, M. Kampmann, T. R. Peterson, K. Nakamura, M. A. Fischbach, J. S. Weissman, L. A. Gilbert, Mapping the Genetic Landscape of Human Cells. *Cell*. **174**, 953-967.e22 (2018).
20. M. Olivieri, T. Cho, A. Álvarez-Quilón, K. Li, M. J. Schellenberg, M. Zimmermann, N. Hustedt, S. E. Rossi, S. Adam, H. Melo, A. M. Heijink, G. Sastre-Moreno, N. Moatti, R. K. Szilard, A. McEwan, A. K. Ling, A. Serrano-Benitez, T. Ubhi, S. Feng, J. Pawling, I. Delgado-Sainz, M. W. Ferguson, J. W. Dennis, G. W. Brown, F. Cortés-Ledesma, R. S. Williams, A. Martin, D. Xu, D. Durocher, A Genetic Map of the Response to DNA Damage in Human Cells. *Cell*. **182**, 481-496.e21 (2020).
21. L. Przybyla, L. A. Gilbert, A new era in functional genomics screens. *Nat. Rev. Genet.* **23**, 89–103 (2022).

22. C. Bock, P. Datlinger, F. Chardon, M. A. Coelho, M. B. Dong, K. A. Lawson, T. Lu, L. Maroc, T. M. Norman, B. Song, G. Stanley, S. Chen, M. Garnett, W. Li, J. Moffat, L. S. Qi, R. S. Shapiro, J. Shendure, J. S. Weissman, X. Zhuang, High-content CRISPR screening. *Nat. Rev. Methods Primer*. **2**, 8 (2022).
23. S. M. Hill, N. K. Nesser, K. Johnson-Camacho, M. Jeffress, A. Johnson, C. Boniface, S. E. F. Spencer, Y. Lu, L. M. Heiser, Y. Lawrence, N. T. Pande, J. E. Korkola, J. W. Gray, G. B. Mills, S. Mukherjee, P. T. Spellman, Context Specificity in Causal Signaling Networks Revealed by Phosphoprotein Profiling. *Cell Syst.* **4**, 73-83.e10 (2017).
24. A. Frost, M. G. Elgort, O. Brandman, C. Ives, S. R. Collins, L. Miller-Vedam, J. Weibezahn, M. Y. Hein, I. Poser, M. Mann, A. A. Hyman, J. S. Weissman, Functional repurposing revealed by comparing S. pombe and S. cerevisiae genetic interactions. *Cell*. **149**, 1339–1352 (2012).
25. M. Costanzo, J. Hou, V. Messier, J. Nelson, M. Rahman, B. VanderSluis, W. Wang, C. Pons, C. Ross, M. Ušaj, B.-J. San Luis, E. Shuteriqi, E. N. Koch, P. Aloy, C. L. Myers, C. Boone, B. Andrews, Environmental robustness of the global yeast genetic interaction network. *Science*. **372**, eabf8424 (2021).
26. J. Tischler, B. Lehner, A. G. Fraser, Evolutionary plasticity of genetic interaction networks. *Nat. Genet.* **40**, 390–391 (2008).
27. S. Bandyopadhyay, M. Mehta, D. Kuo, M.-K. Sung, R. Chuang, E. J. Jaehnig, B. Bodenmiller, K. Licon, W. Copeland, M. Shales, D. Fiedler, J. Dutkowski, A. Guénolé, H. van Attikum, K. M. Shokat, R. D. Kolodner, W.-K. Huh, R. Aebersold, M.-C. Keogh, N. J. Krogan, T. Ideker, Rewiring of genetic networks in response to

DNA damage. *Science*. **330**, 1385–1389 (2010).

28. S. P. Jackson, J. Bartek, The DNA-damage response in human biology and disease. *Nature*. **461**, 1071–1078 (2009).
29. L. A. Gilbert, M. A. Horlbeck, B. Adamson, J. E. Villalta, Y. Chen, E. H. Whitehead, C. Guimaraes, B. Panning, H. L. Ploegh, M. C. Bassik, L. S. Qi, M. Kampmann, J. S. Weissman, Genome-Scale CRISPR-Mediated Control of Gene Repression and Activation. *Cell*. **159**, 647–661 (2014).
30. M. A. Horlbeck, L. A. Gilbert, J. E. Villalta, B. Adamson, R. A. Pak, Y. Chen, A. P. Fields, C. Y. Park, J. E. Corn, M. Kampmann, J. S. Weissman, Compact and highly active next-generation libraries for CRISPR-mediated gene repression and activation. *eLife*. **5**, e19760 (2016).
31. S. Ruiz, C. Mayor-Ruiz, V. Lafarga, M. Murga, M. Vega-Sendino, S. Ortega, O. Fernandez-Capetillo, A Genome-wide CRISPR Screen Identifies CDC25A as a Determinant of Sensitivity to ATR Inhibitors. *Mol. Cell*. **62**, 307–313 (2016).
32. C. Wang, G. Wang, X. Feng, P. Shepherd, J. Zhang, M. Tang, Z. Chen, M. Srivastava, M. E. McLaughlin, N. M. Navone, G. T. Hart, J. Chen, Genome-wide CRISPR screens reveal synthetic lethality of RNASEH2 deficiency and ATR inhibition. *Oncogene*. **38**, 2451–2463 (2019).
33. N. Y. L. Ngoi, M. M. Pham, D. S. P. Tan, T. A. Yap, Targeting the replication stress response through synthetic lethal strategies in cancer medicine. *Trends Cancer*. **7**, 930–957 (2021).
34. H. Goto, T. Natsume, M. T. Kanemaki, A. Kaito, S. Wang, E. C. Gabazza, M. Inagaki, A. Mizoguchi, Chk1-mediated Cdc25A degradation as a critical

mechanism for normal cell cycle progression. *J. Cell Sci.* **132**, jcs223123 (2019).

35. T. M. Norman, M. A. Horlbeck, J. M. Replogle, A. Y. Ge, A. Xu, M. Jost, L. A. Gilbert, J. S. Weissman, Exploring genetic interaction manifolds constructed from rich single-cell phenotypes. *Science*. **365**, 786–793 (2019).
36. I. Garcia-Higuera, T. Taniguchi, S. Ganesan, M. S. Meyn, C. Timmers, J. Hejna, M. Grompe, A. D. D'Andrea, Interaction of the Fanconi anemia proteins and BRCA1 in a common pathway. *Mol. Cell*. **7**, 249–262 (2001).
37. K. Townsend, H. Mason, A. N. Blackford, E. S. Miller, J. R. Chapman, G. G. Sedgwick, G. Barone, A. S. Turnell, G. S. Stewart, Mediator of DNA damage checkpoint 1 (MDC1) regulates mitotic progression. *J. Biol. Chem.* **284**, 33939–33948 (2009).
38. A. Ghelli Luserna di Rorà, C. Cerchione, G. Martinelli, G. Simonetti, A WEE1 family business: regulation of mitosis, cancer progression, and therapeutic target. *J. Hematol. Oncol.J Hematol Oncol*. **13**, 126 (2020).
39. F. Merolla, C. Luise, M. T. Muller, R. Pacelli, A. Fusco, A. Celetti, Loss of CCDC6, the first identified RET partner gene, affects pH2AX S139 levels and accelerates mitotic entry upon DNA damage. *PloS One*. **7**, e36177 (2012).
40. Y. Sun, X. Jiang, S. Chen, N. Fernandes, B. D. Price, A role for the Tip60 histone acetyltransferase in the acetylation and activation of ATM. *Proc. Natl. Acad. Sci. U. S. A.* **102**, 13182–13187 (2005).
41. M. Ikura, K. Furuya, S. Matsuda, R. Matsuda, H. Shima, J. Adachi, T. Matsuda, T. Shiraki, T. Ikura, Acetylation of Histone H2AX at Lys 5 by the TIP60 Histone Acetyltransferase Complex Is Essential for the Dynamic Binding of NBS1 to

Damaged Chromatin. *Mol. Cell. Biol.* **35**, 4147–4157 (2015).

42. T. Procida, T. Friedrich, A. P. M. Jack, M. Peritore, C. Bönisch, H. C. Eberl, N. Daus, K. Kletenkov, A. Nist, T. Stiewe, T. Borggrefe, M. Mann, M. Bartkuhn, S. B. Hake, JAZF1, A Novel p400/TIP60/NuA4 Complex Member, Regulates H2A.Z Acetylation at Regulatory Regions. *Int. J. Mol. Sci.* **22**, E678 (2021).
43. X. Wang, S. Ahmad, Z. Zhang, J. Côté, G. Cai, Architecture of the Saccharomyces cerevisiae NuA4/TIP60 complex. *Nat. Commun.* **9**, 1147 (2018).
44. P. Nghiem, P. K. Park, Y. Kim, C. Vaziri, S. L. Schreiber, ATR inhibition selectively sensitizes G1 checkpoint-deficient cells to lethal premature chromatin condensation. *Proc. Natl. Acad. Sci. U. S. A.* **98**, 9092–9097 (2001).

Publishing Agreement

It is the policy of the University to encourage open access and broad distribution of all theses, dissertations, and manuscripts. The Graduate Division will facilitate the distribution of UCSF theses, dissertations, and manuscripts to the UCSF Library for open access and distribution. UCSF will make such theses, dissertations, and manuscripts accessible to the public and will take reasonable steps to preserve these works in perpetuity.

I hereby grant the non-exclusive, perpetual right to The Regents of the University of California to reproduce, publicly display, distribute, preserve, and publish copies of my thesis, dissertation, or manuscript in any form or media, now existing or later derived, including access online for teaching, research, and public service purposes.

DocuSigned by:
Benjamin Herken
C6FA0534941948B...
Author Signature

3/14/2023
Date